Precambrian Research 311 (2018) 157–166

Contents lists available at ScienceDirect

Precambrian Research

journal homepage: www.elsevier.com/locate/precamres

Highly heterogeneous "poikiloredox" conditions in the early Ediacaran Yangtze Sea

Chengsheng Jin[a,b,c], Chao Li[c,*], Thomas J. Algeo[d,e], Brennan O'Connell[f], Meng Cheng[c], Wei Shi[c], Jun Shen[d], Noah J. Planavsky[f]

[a] Yunnan Key Laboratory for Palaeobiology, Yunnan University, Kunming 650091, China
[b] MEC International Joint Laboratory for Palaeobiology & Palaeoenvironment, Yunnan University, Kunming 650091, China
[c] State Key Laboratory of Biogeology and Environmental Geology, China University of Geosciences, Wuhan 430074, China
[d] State Key Laboratory of Geological Processes and Mineral Resources, China University of Geosciences, Wuhan 430074, China
[e] Department of Geology, University of Cincinnati, Cincinnati, OH 45221-0013, USA
[f] Department of Geology and Geophysics, Yale University, New Haven, CT 06520, USA

ARTICLE INFO

Keywords:
Iron speciation
Oxygen
Trace elements
Molybdenum
Uranium
Phosphorus

ABSTRACT

Although there has been a sustained effort to reconstruct ocean-redox conditions throughout the Ediacaran, a lack of high-resolution data across time-equivalent strata (shelf to basin) has hindered our ability to understand redox dynamics at the basinal scale. We measured iron species, trace- and major-element concentrations, TOC, and C_{org}/P ratios of black shale from six high-resolution sections from the early Ediacaran Yangtze Sea (i.e., the inner-shelf Jiulongwan, outer-shelf Zhongling, slope Siduping and Mingle, and basinal Yuanjia and Long'e sections), which were integrated with published data from these sections and seven other correlative sections from the same region for a basinwide perspective on redox tracers. These results document strong spatio-temporal redox variability during the early Ediacaran, including transitions between ferruginous, euxinic, suboxic, and oxic conditions at high frequencies and short distances (a pattern for which we coin the term "poikiloredox conditions"). Our results also suggest that multiple geochemical proxies including iron species, redox sensitive trace element concentrations and enrichments, and C_{org}/P ratios show different responses to poikiloredox conditions, accounting for conflicting redox interpretations in early Ediacaran studies. This study thus demonstrates the importance of multiple proxies, high stratigraphic resolution, and a basin-scale perspective in paleomarine redox studies, underlining the potential for overgeneralization of redox patterns based on analysis of a single or a limited number of proxies or sections.

1. Introduction

The oxygenation of the Earth's ocean-atmosphere system represents one of the most dramatic transitions in Earth history. A consensus view on the redox conditions of Archean and Phanerozoic oceans has emerged: Archean oceans were largely anoxic except for local surface waters (e.g., Reinhard et al., 2013), whereas Phanerozoic oceans were well-oxygenated with the exception of anoxic isolated basins and oxygen-minimum zones of continental margins. Over the past five years, there has been a flood of over 100 papers focused on Proterozoic redox conditions. Despite these efforts, the debate about the redox structure of the transitional Proterozoic ocean remains unresolved (cf. Lyons et al., 2014). Studies using different redox methods have yielded widely contrasting views, with some inferring rapid swings in marine oxygen levels (e.g., Sahoo et al., 2012, 2016) and others advocating no measurable changes (e.g., Sperling et al., 2015; Miller et al., 2017). Some redox features of Proterozoic ocean systems—for example, a mid-depth euxinic wedge (e.g., Li et al., 2010)—have been inferred based on observations from multiple sections. Higher-resolution spatial and temporal sampling of time-equivalent sections may help resolve these contradictions and move us towards a more complete understanding of basin-scale redox dynamics.

One of the key tools used to track secular changes in atmospheric and oceanic oxygen levels through time is levels of enrichment of redox-sensitive trace elements (RSTEs) relative to organic carbon (RSTE/TOC) in anoxic marine shales (e.g., Scott et al., 2008; Sahoo et al., 2012). Following the development of pervasive oxidative weathering during the 'Great Oxidation Event' beginning at ~2.4 Ga, the oceanic inventory of RSTEs primarily depended on the relative spatial extent of anoxic to oxic conditions in global seawater (Scott

* Corresponding author.
E-mail address: chaoli@cug.edu.cn (C. Li).

https://doi.org/10.1016/j.precamres.2018.04.012
Received 13 January 2018; Received in revised form 5 April 2018; Accepted 13 April 2018
Available online 15 April 2018

et al., 2008). Because most RSTEs are removed to the sediment at higher rates under reducing conditions compared to oxidizing conditions, seawater RSTE concentrations are thought to have increased through time in response to rising oceanic oxygen levels. Long-term changes in the oceanic inventory of RSTEs can be reflected in their degree of enrichment in organic-rich anoxic facies (e.g., Scott et al., 2008). Furthermore, the long residence times of some RSTEs (e.g., Mo: ~780 kyr; U: ~450 kyr; V: ~50 kyr) compared to oceanic mixing times (~1–2 kyr) make them particularly useful for tracking global-oceanic redox conditions (e.g., Emerson and Huested, 1991). However, RSTE enrichment levels vary widely in modern anoxic marine environments owing to the influences of sedimentation rates, organic matter fluxes, and sulfide levels. In this light, a basin-scale perspective is essential for evaluation of the significance of trace-metal enrichments.

A rapid rise in RSTE concentrations within the basal Doushantuo Formation of South China to levels comparable to those of Phanerozoic anoxic facies has been interpreted as evidence for a well-oxygenated deep ocean in the early Ediacaran, possibly linked to oxygenation triggered by the Marinoan Snowball Earth glaciation (Sahoo et al., 2012). This view was challenged by Miller et al. (2017), who argued that RSTE enrichment of anoxic shales in South China was primarily a local phenomenon (e.g., related to hydrothermal fluids or exceptionally low sedimentation rates) because of the absence of similar patterns in correlative sections in Svalbard and Canada. However, the hydrothermal overprinting interpretation clashes with laser ablation work on trace-metal concentrations in pyrite and the preservation of depositional sulfide texture (e.g., framboidal pyrite) in the Doushantuo Formation (Gregory et al., 2017). Here, we provide a new perspective on this debate by exploring RSTEs of the basal Doushantuo Formation in multiple sections representing two shallow-to-deep transects in South China.

Given the importance of South China sections in shaping our view of early Ediacaran ocean-redox conditions, we decided to undertake a comprehensive redox study making use of multiple geochemical proxies at high spatial and temporal resolutions. To this end, we (1) analyzed Fe species ratios, RSTE concentrations and enrichment factors, and C_{org}/P ratios at six locales on the Yangtze Block (i.e., the inner-shelf Jiulongwan, outer-shelf Zhongling, slope Siduping and Mingle, and basinal Yuanjia and Long'e sections); (2) compiled published data for the same geochemical proxies from these sections and seven other early Ediacaran sections from the same region; and (3) generated two shelf-to-basin transects that were used to evaluate spatiotemporal variation in redox conditions across the Yangtze Block. This analysis was conducted within a well-established, high-resolution correlation framework for the Ediacaran of South China (Jiang et al., 2010, 2011), making possible detailed assessments of secular relationships among the study sections. Our study provides two key insights: 1) high spatiotemporal redox variability (including ferruginous, euxinic, suboxic, and oxic conditions) existed across the Yangtze Block during the early Ediacaran, and 2) multiple geochemical proxies including iron species, RSTE concentrations and enrichments, and C_{org}/P ratios exhibited differential responses to high-frequency redox fluctuations.

2. Geological setting

During the early Ediacaran, the South China Craton was an isolated microcontinent at mid-latitudes of the Northern Hemisphere (Fig. 1A; Zhang et al., 2013). It consisted of the Yangtze Block to the northwest and the Cathaysia Block to the southeast (modern coordinates), separated by the deepwater Nanhua Basin (Fig. 1B), which had developed as a failed rift basin at ~820 Ma (Wang and Li, 2003). The water depth of the Nanhua Basin on the Yangtze Block where all study sections were located increased from northwest (shelf facies) to southeast (basinal facies) (Fig. 1B). Although a non-marine (lacustrine) depositional setting was proposed for the early Ediacaran Nanhua Basin based on the ubiquitous occurrence of saponite (Bristow et al., 2009), this mineral is equally likely to have been the detrital product of weathering of mafic and ultramafic volcanic rocks or to have formed within marine sediments (Huang et al., 2013). Several lines of evidence point towards a connection of the Nanhua Basin to the contemporaneous global ocean: (1) South China was an isolated craton surrounded by deep-water areas (Fig. 1A; Zhang et al., 2013); (2) cap carbonate and overlying black shale deposits in South China are similar to those in coeval sections globally (Jiang et al., 2011), and (3) acritarch biotas in South China and elsewhere are globally cosmopolitan at this time (Zhou et al., 2007).

The lower Ediacaran succession comprises Members I and II of the Doushantuo Formation, which overlies the Cryogenian Nantuo Formation (Fig. 1C). Member I consists of cap carbonate, the basal part of Member II consists mainly of black shale, and the upper part of Member II consists of silty or shaly dolostone or dolomitic siltstone (Jiang et al., 2010, 2011). The stratigraphic package of cap carbonates overlain by black shales serves as a regional stratigraphic marker across the Yangtze Block that can even be correlated globally (Jiang et al., 2011). At Jiulongwan, the black shale contains abundant acanthomorphic acritarchs such as *Tianzhushania spinosa*, *Apodastoides basileus*, *Meghystrichosphaeridium perfectum*, *Eotyotopalla dactylos*, *Ericiasphaera magna*, *Eotyotopalla delicata*, *Meghystrichosphaeridium magnificum,* and *Tianzhushania conoideum*, but no fossils have been reported from the other five study sections (McFadden et al., 2009).

The black shale of the lower part of Member II is a 4- to 5-m-thick unit deposited during the late deglacial transgression following the Marinoan glaciation (Fig. 1C; Jiang et al., 2011). The lithologic shift from cap carbonate to black shale was transitional and conformable, as suggested by numerous thin carbonate beds or nodule layers within the black shale at the shelf-slope break (Jiang et al., 2010). Some shale beds from the outer-shelf Zhongling, slope Siduping, and basinal Yiuanjia sections are characterized by alternating gray and black layers of < 1 cm thickness (Fig. 2; Jiang et al., 2010). The black shale is thinly laminated without any evidence for wave or storm activity, suggesting deposition below storm wavebase (Jiang et al., 2010). Deposition of the black shale unit began around ca. 635 Ma, based on zircon U-Pb ages of 635.2 ± 0.6 Ma and 632.5 ± 0.5 Ma from ash beds within Member I at Wuhe and Member II at Jijiawan, respectively (Condon et al., 2005). These ages yield an average sedimentation rate of ~2 m/Myr for the 6-m interval between the dated horizons (Fig. 1C). The age of the top of the black shale interval is poorly constrained.

3. Materials and methods

We analyzed redox tracers in six sections from the early Ediacaran Yangtze Sea, all of which except Siduping have been the subject of earlier geochemical studies. We generated Fe-C-Al-P-trace metal data, as needed for each section, to develop an integrated, complete paleoredox dataset (Table S1). Integrated data sources for the six study sections are: (1) inner-shelf Jiulongwan (Li et al., 2010; Och et al., 2016; this study), (2) outer-shelf Zhongling (Li et al., 2010; this study), (3) slope Siduping (Wang et al., 2012; this study), (4) slope Mingle (Li et al., 2010; this study), (5) basinal Yuanjia (Sahoo et al., 2012; this study), and (6) basinal Long'e (Li et al., 2010; this study). In addition, we compiled the same types of redox data for an additional seven sections on the Yangtze Block from previously published sources: (1) inner-shelf Jiuqunao (Och et al., 2016), (2) outer-shelf Weng'an (Sahoo, 2015), (3) slope Rongxi (Sahoo, 2015), (4) slope Daotuo (Ye et al., 2017; Zhai et al., 2018), (5) slope Taoying (Sahoo et al., 2012), (6) basinal Wuhe (Sahoo et al., 2012), and (7) Xiangtan (Han and Fan, 2015). These 13 sections were used to construct two intersecting paleoredox cross-sections across the early Ediacaran Yangtze Block (Fig. 1B).

Fresh samples were collected from each section for geochemical analyses, and any weathered surfaces, post-depositional veins, and visible pyrite crystals were removed prior to powdering. The selected samples were cut into small pieces and then crushed to powder using a

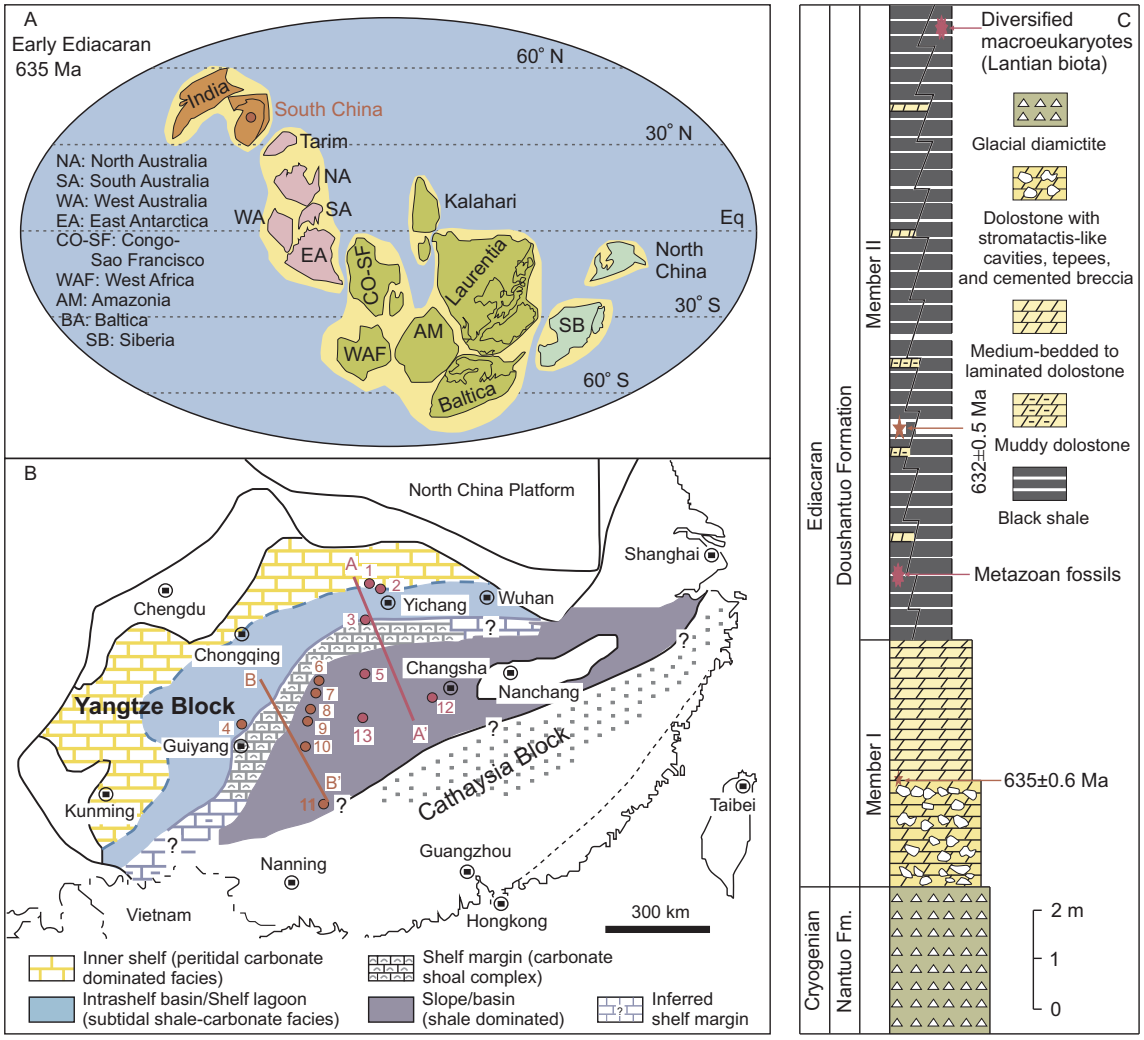

Fig. 1. Geological background for the study sections. (A) Global paleogeography showing the location of South China at ~635 Ma (Zhang et al., 2013). (B) General paleogeography of the Yangtze Platform (i.e., Nanhua Basin) during the deposition of Doushantuo Formation (Jiang et al., 2011) and the locations of study sections in the Nanhua Basin. The study sections mentioned in the text are marked in pink (Transect A-A′) and red (Transect B-B′) dots. Sections: 1-Jiuqunao, 2-Jiulongwan, 3-Zhongling, 4-Weng'an, 5-Siduping, 6-Mingle, 7-Rongxi, 8-Daotuo, 9-Taoying, 10-Wuhe, 11-Long'e, 12-Xiangtan, and 13-Yuanjia. (C) General stratigraphy of basal Doushantuo Formation (Jiang et al., 2011). U-Pb ages of 635.2 ± 0.6 Ma and 632.5 ± 0.5 Ma are from ash beds within Member I at Wuhe and Member II at Jijiawan, respectively (Condon et al., 2005). Fossil records are based on McFadden et al. (2009) and Yuan et al. (2011).

vibrating disc mill (Retsch RS200). All analytical work was performed at the State Key Laboratory of Biogeology and Environmental Geology, China University of Geosciences (Wuhan).

Highly reactive iron (Fe_{HR}) is the sum of iron in four different pools: carbonate iron (Fe_{carb}), oxide iron (Fe_{ox}), magnetite iron (Fe_{mag}), and pyrite iron (Fe_{py}). The first three iron species were measured using a sequential extraction procedure described by Poulton and Canfield (2005). About 100 mg of sample powder were treated at 50 °C for 48 h in a sodium acetate solution adjusted to a pH of 4.5 by addition of analytical-grade acetic acid to extract Fe_{carb}. The residual sample from the first step was treated at room temperature for 2 h in a 50-g/L sodium dithionite solution adjusted to a pH of 4.8 by addition of 0.2-M sodium citrate and analytical-grade acetic acid to extract Fe_{ox}. The residual sample from the second step was further treated at room temperature for 6 h in a 0.2-M ammonium oxalate and 0.17-M oxalic acid solution adjusted to a pH of 3.2 by addition of analytical-grade ammonia water to extract Fe_{mag}. All extracts were diluted by 2% nitric acid, and Fe contents were determined using an atomic absorption spectroscope (AAS) with a RSD of < 5%. Two laboratory shale standards (CUG-2 and CUG-3) were used for quality control of the sequential extraction with standard deviation of measured values from the expected values ≤0.03% for CUG-2 and ≤0.15% for CUG-3 (Li et al., 2015a). Fe_{py} was calculated stoichiometrically based on pyrite sulfur recovered using the Cr-reduction method (Canfield et al., 1986). Sample powders were treated under N_2 with 20 ml of 12-N HCl and 40 ml of 1-M chromous chloride solution and heated for 2 h. The liberated hydrogen sulfide was precipitated as Ag_2S by addition of 30 ml of 3% silver nitrate and 10% ammonia water. The Ag_2S precipitate was then filtered, rinsed, dried, and weighed.

Trace element concentrations were measured using an Agilent 7500a quadrupole inductively coupled plasma mass spectrometry (ICP-MS). Prior to analysis, sample powders were ashed at 850 °C for 8 h to remove volatiles. Then, about 50 mg of each ashed sample were dissolved at 200 °C in a 15-ml Teflon bomb by sequential addition of HNO_3, HNO_3-HF (1:2), and HCl (Li et al., 2010). Following complete digestion, the concentrated acid was then removed through evaporation. Finally, each sample was diluted with 2% nitric acid and analyzed for trace elements using the ICP-MS. Analytical errors were better than ± 5% for trace elements on the basis of USGS (BCR-2) and Chinese national standards (GBW07103, GBW07104). Enrichment factors (EF) for trace elements were calculated as: $X_{EF} = (X/Y)_{sample}/(X/Y)_{AUCC}$, in which X and Y are the trace element of interest (e.g., Mo, U,

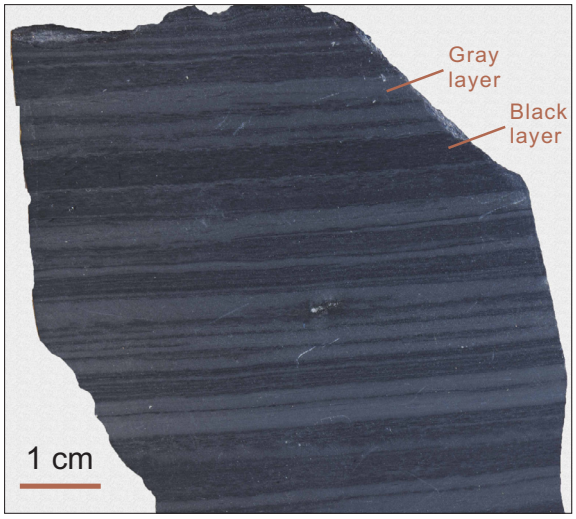

Fig. 2. Alternating gray and black layers in a ~6-cm-thick interval from the lower part of the Doushantuo Member II of the basinal Yuanjia section. This lithological variation reflects high-frequency paleoredox fluctuations.

or V) and a conservative major element used for normalization (i.e., Al or Ti), respectively, and AUCC = average upper continental crust (McLennan, 2001).

Major element concentrations were determined using PANalytical Epsilon 3X X-ray fluorescence spectrometry (XRF). About 0.6 g of sample powder, 6 g of a $Li_2B_4O_7$-$LiBO_2$-LiF mixture, and 0.3–0.4 g of ammonium nitrate were sequentially weighed into a porcelain crucible and then completely mixed. The mixture was transferred into a platinum crucible with the addition of about 5 drops of lithium bromide solution, and the mixture was then placed in a fusion machine at 1080 °C for 10 min to produce a glass bead. The glass bead was analyzed for targeted major elements (Fe_T, Al, and P) using the PANalytical Epsilon 3X XRF instrument. Analytical errors were better than ± 5% for major elements on the basis of replicate analyses of two Chinese national standards (GBW07107 and GBW07108).

Aliquots of sample powders for analysis of total organic carbon (TOC) were decarbonated with HCl, rinsed, and buffered to a pH of 7.0 using distilled water. The residual samples were dried and then combusted under a pure O_2 atmosphere at 1350 °C for 6 min to liberate carbon as CO_2, which was measured using a Jena Multi-EA 4000 carbon-sulfur analyzer. Analytical errors were better than ± 0.2% on the basis of repeated analysis of an Alpha Resources standard (AR 4007).

4. Background: Geochemical proxies for paleo-redox conditions

Aqueous environments are classified on the basis of dissolved O_2 and H_2S concentrations as oxic ($> 2\,ml\,O_2\,L^{-1}$), suboxic ($0.2–2\,ml\,O_2\,L^{-1}$), or anoxic ($0–0.2\,ml\,O_2\,L^{-1}$), with the last category divided into anoxic-ferruginous (aqueous Fe(II) present; no H_2S) or euxinic (H_2S present; no aqueous Fe(II)) (Tyson and Pearson, 1991; Poulton and Canfield, 2011). These redox facies were likely consequences of aerobic respiration (oxic), nitrate, and manganese (suboxic), iron reduction (ferruginous), sulfate reduction (euxinic), and methanogenesis (ferruginous) in the early oxidant-controlled redox-stratified oceans (Li et al., 2015b). It should be noted that many depositional systems are subject to frequent redox fluctuations (Algeo and Ingall, 2007), and therefore redox proxies can do no more than give an approximation of time-averaged conditions. Furthermore, different redox proxies often respond in a non-uniform manner to high-frequency redox fluctuations in such systems, yielding apparent contradictions (e.g., Cheng et al., 2017; Lei et al., 2017; see Section 5.2).

Sedimentary iron proxies—foremost iron species—are the most commonly used local redox proxies in the Proterozoic. Iron speciation relies on linking the distribution and abundance of biogeochemically reactive iron minerals (e.g., authigenic Fe-bearing minerals such as pyrite and magnetite) in marine sediments to redox conditions, and the method is empirically calibrated based on extensive study of modern or Phanerozoic marine sediments. The largest source of uncertainty in this procedure is ensuring that the analyzed samples are comparable to those used for proxy calibration (i.e., typical continental margin mudstones, although carbonates have also recently been explored; e.g., Clarkson et al., 2014). This agreement can be difficult to establish with confidence, especially in the analysis of billon-year-old rocks. Recently, it has been noted that iron is mobile and reactive during diagenesis, and thus post-depositional processes can overprint primary Fe-speciation redox signatures (Slotznick et al., 2018). For example, a wide range of Fe_{py}/Fe_{HR} and Fe_{HR}/Fe_T ratios were documented in a Silurian-Devonian sedimentary succession that underwent regional metamorphism from lower greenschist facies to granulite facies (Slotznick et al., 2018). The generated Fe speciation data were interpreted to indicate variably oxic, ferruginous, and euxinic conditions, but global and local biological constraints pointed instead toward well-oxygenated conditions (Slotznick et al., 2018). Interpretations of iron proxy data are often viewed within a framework of threshold values established from modern/Phanerozoic sediments. Sediments having $Fe_{HR}/Fe_T > 0.38$ represent anoxic conditions (Raiswell and Canfield, 1998), which can be further characterized as either ferruginous or euxinic conditions based on Fe_{Py}/Fe_{HR} ratios that are respectively smaller or > 0.7–0.8 (note: the threshold is slightly indeterminate) (Poulton and Canfield, 2011). These threshold values are considered to be effective for siliciclastic rocks (Lyons and Severmann, 2006) and for carbonate rocks with $Fe_T > 0.5\%$ (Clarkson et al., 2014).

Redox-sensitive trace elements (RSTEs) can also be used to infer paleo-redox conditions (Algeo and Maynard, 2004; Tribovillard et al., 2006). Molybdenum (Mo) is present mainly as the conservative molybdate anion (MoO_4^{2-}) in oxic waters, but it is converted to particle-reactive thiomolybdates ($MoO_{4-x}S_x^{2-}$, x = 1–4) in the presence of H_2S and rapidly scavenged to the sediment through adsorption onto organic matter and/or formation of sulfide minerals. U is present mainly as the conservative U(VI) species in oxic waters, but it is reduced to U(IV) under suboxic (Fe-reducing) to anoxic conditions and removed to the sediment as UO_2. V is present as V(V) in oxic waters, but it is reduced first to V(IV) and then to V(III) under progressively more reducing conditions, leading to more rapid uptake by the sediment. In the modern ocean, these RSTEs show little to no authigenic enrichment in oxic depositional facies but strong enrichment in euxinic facies (to enrichment factors, or EFs, > 100; Tribovillard et al., 2006). However, RSTE enrichments are influenced by basin hydrography, with less enrichment in strongly restricted basins such as the modern Black Sea (Algeo and Lyons, 2006), and by the size of the oceanic RSTE reservoir, which was lower during the Precambrian when oxidative weathering or RSTEs was limited and widespread oceanic anoxia facilitated removal of RSTEs to the sediment at a global scale (Scott et al., 2008).

Phosphorus (P) retention in sediments has been suggested as a redox proxy (C_{org}/P ratios are < ~50:1 for oxic conditions, ~50:1 to ~100:1 for suboxic conditions, and > ~100:1 for anoxic conditions; Algeo and Ingall, 2007). However, there are significant uncertainties associated with this proxy. Although redox conditions in bottomwaters and surface sediment porewaters can influence P burial efficiency in siliciclastic sediments (e.g., Ingall et al., 1993), P enrichment in shales is not entirely governed by redox conditions, and both anoxic and oxic sediments can show similar enrichment levels (Reinhard et al., 2017). Furthermore, other factors, such as organic matter loading and local variations in sedimentation rate, can also play a key role in determining P enrichment of the sediment. For example, P levels in sediment porewaters depend on the extent of organic matter loading and organic matter decomposition. The burial flux of carbon is related to the depositional flux to the sediment-water interface and burial efficiency,

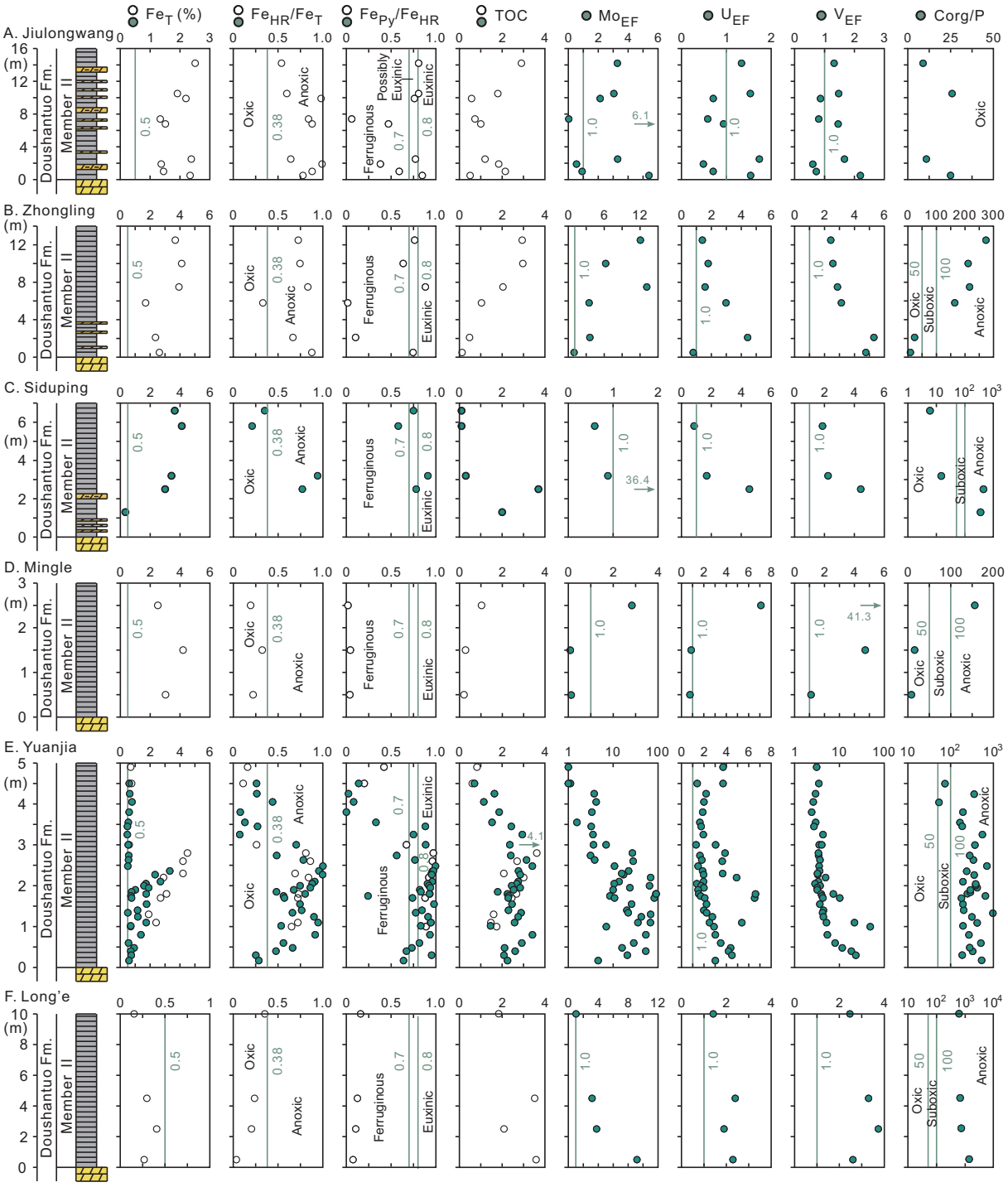

Fig. 3. Integrated chemostratigraphy of the basal Doushantuo Formation in Jiulongwan (A), Zhongling (B), Siduping (C), Mingle (D), Yuanjia (E) and Long'e (F) sections. The vertical line(s) in each profile represents key threshold value(s) discussed in text. Data original to this study are shown by solid symbols, and data from published sources by open symbols. Published data from Li et al. (2010) for Jiulongwan, Zhongling, Mingle, and Long'e; Och et al. (2016) for Jiulongwan; and Sahoo et al. (2012) for Yuanjia.

which is dependent on sedimentation rate. This in turn will regulate the amount of P available in the porewaters for carbonate fluorapatite precipitation. Burial of authigenic carbonate fluorapatite is the largest burial flux of P in the modern oceans—accounting for at least half of all reactive P burial (e.g., Filippelli, 2002; Ruttenberg, 2003). Therefore, although we utilize this proxy, we embrace the likelihood that C_{org}/P ratios are not likely as robust redox indicators as Fe speciation and RSTEs.

5. Results and discussion

5.1. General redox interpretations for the study sections

In the inner-shelf Jiulongwan section (Fig. 3A; Table S1), all samples are characterized by $Fe_T > 0.5\%$, high Fe_{HR}/Fe_T (0.54–0.99), and variable Fe_{Py}/Fe_{HR} (0.06–0.85), indicating ferruginous to euxinic conditions. However, this section is characterized by relatively low RSTE enrichments ($Mo_{EF} = 2.8 \pm 2.1$, $U_{EF} = 1.1 \pm 0.5$, and

V_{EF} = 1.2 ± 0.5; all cited proxy values are either ranges or means plus/minus one standard deviation). These low EFs could be indicative of oxic conditions or rapid sedimentation. Low C_{org}/P ratios (18 ± 9), have been suggested to record oxic conditions (Algeo and Ingall, 2007), in agreement with RSTE enrichments but not iron speciation. Furthermore, large (> 10 μm) pyrite framboids hint at sulfidic porewaters and early diagenetic pyrite formation (Sahoo, 2015), which rules out euxinic deposition but not deposition under ferruginous conditions. Collectively, the measured redox proxies suggest a conflicting redox history at Jiulongwan, with redox conditions between ferruginous and oxic conditions.

In the outer-shelf Zhongling section (Fig. 3B; Table S1), all samples show Fe_T > 0.5%, variable Fe_{HR}/Fe_T (0.33–0.87), and variable Fe_{Py}/Fe_{HR} (0.02–0.88), suggesting widely varying (i.e., oxic-ferruginous-euxinic) redox conditions. Trace metals show modest enrichments (Mo_{EF} = 6.6 ± 4.9, U_{EF} = 2.2 ± 1.3, and V_{EF} 3.5 ± 1.2), indicative of suboxic conditions. C_{org}/P ratios (150 ± 109), have been suggested to record suboxic to weakly euxinic conditions (Algeo and Ingall, 2007), similar to redox estimates from RSTE enrichments (suboxic) and few iron speciation measurements (euxinic). Similar to inner-shelf (Jiulongwan section) environments, a redox conditions in the outer-shelf environments at Zhongling appear to be variable and some samples again yield conflicting redox signatures.

In the slope Siduping section (Fig. 3C; Table S1), all samples except for one with low Fe_T content are characterized by Fe_T > 0.5%, low to high Fe_{HR}/Fe_T (0.21–0.94), and moderate to high Fe_{Py}/Fe_{HR} (0.58–0.91), suggesting widely varying (i.e., oxic to euxinic) redox conditions. Trace metals show modest enrichments (Mo_{EF} = 12.6 ± 20.6, U_{EF} = 2.4 ± 1.9, and V_{EF} = 2.8 ± 1.4), indicative of suboxic conditions. By contrast, C_{org}/P ratios (mean 185, range 10–408), have been suggested to indicate of dominantly euxinic but fluctuating redox conditions. C_{org}/P ratios, do not agree with RSTE enrichment data, and are only compatible with a few of the iron speciation data. Conflicting redox conditions are, again, indicated by Fe speciation data and RSTE enrichments for slope environments at Siduping.

In the slope Mingle section (Fig. 3D; Table S1), two of three samples are characterized by Fe_T > 0.5%, low Fe_{HR}/Fe_T (0.22–0.32), and low Fe_{Py}/Fe_{HR} (0.04–0.05), indicating oxic conditions, an inference that is supported by low Mo_{EF} (0.1 ± 0.0), U_{EF} (0.8 ± 0.1), V_{EF} (2.9 ± 2.6). C_{org}/P ratios (12 ± 5) also agree with oxic conditions inferred by iron speciation and RSTE enrichments. For the third sample, low Fe_{HR}/Fe_T (0.19) and low Fe_{Py}/Fe_{HR} (0.02) imply oxic conditions, but trace-metal enrichments (Mo_{EF} = 2.8, U_{EF} = 7.1, and V_{EF} = 41.3) and an elevated C_{org}/P ratio (156) are indicative of suboxic to anoxic conditions. In the slope setting Mingle section, redox proxies indicated by three redox proxies are generally in agreement with each other.

In the basinal Yuanjia section (Fig. 3E; Table S1), all samples except for two with low Fe_T contents show Fe_T > 0.5%, variable Fe_{HR}/Fe_T (0.08–1.00) and Fe_{Py}/Fe_{HR} (0–0.99), suggesting widely varying (i.e., oxic-ferruginous-euxinic) redox conditions. This interpretation is supported by highly variable trace-metal enrichments (Mo_{EF} = 26.0 ± 26.5, U_{EF} = 2.8 ± 1.4, and V_{EF} = 6.8 ± 8.6). Fe speciation data and RSTE enrichments do not agree with persistently high C_{org}/P ratios (326 ± 184) indicative of dominantly anoxic conditions.

In the basinal Long'e section (Fig. 3F; Table S1), all samples exhibit Fe_T < 0.5%, obviating the use of iron speciation data for evaluation of local redox conditions. Small enrichments of trace metals (Mo_{EF} = 4.3 ± 3.5, U_{EF} = 2.0 ± 0.4, and V_{EF} = 3.0 ± 0.6) imply suboxic conditions. In contrast, high C_{org}/P ratios (900 ± 384) are indicative of strongly anoxic conditions. Again, redox conditions determined by RSTE enrichments and C_{org}/P ratios are not in agreement.

Differences in redox interpretations based on different proxies are also apparent for the previously studied Jiuqunao (Och et al., 2016), Weng'an (Sahoo, 2015), Rongxi (Sahoo, 2015), Daotuo (Ye et al., 2017; Zhai et al., 2018), Taoying (Sahoo et al., 2012), Wuhe (Sahoo et al., 2012), and Xiangtan (Han and Fan, 2015) sections. For example, some samples from the slope Mingle and Taoying and basinal Wuhe and Yuanjia sections are characterized by low Fe_{HR}/Fe_T (< 0.38), suggesting oxic conditions, and high Mo_{EF} (up to 27.1), U_{EF} (up to 7.2), V_{EF} (up to 59.9) suggesting suboxic to euxinic conditions. Some samples from the inner-shelf Jiuqunao and Jiulongwan and outer-shelf Zhongling sections are characterized by Fe_{HR}/Fe_T > 0.38, suggesting anoxic conditions, but also show low RSTE enrichments (EF < 1), consistent with oxic conditions. Moreover, redox conditions indicated by Fe speciation data and RSTE enrichments are also not in full agreement with C_{org}/P ratios (after Algeo and Ingall, 2007). For example, C_{org}/P ratios > 50 from the Mingle, Taoying, Wuhe and Yuanjia sections suggest suboxic to euxinic conditions, whereas C_{org}/P ratios < 50 from the Jiuqunao, Jiulongwan and Zhongling sections suggest oxic conditions based on the parameters established by Algeo and Ingall (2007). In short, C_{org}/P ratios do not correlate well with RSTE enrichments or Fe speciation data. Similar conflicts in redox interpretations among the proxies have been reported previously for the early Cambrian (Cheng et al., 2017) and Permian-Triassic transition (Lei et al., 2017). The frequency with which such conflicting redox interpretations appear is a caveat against making broad-scale redox interpretations based on a single proxy or section (e.g., Scheller et al., 2017).

5.2. Causes of conflicting redox interpretations for the study sections

The conflicting redox interpretations indicated above are likely to be, in part, a consequence of the differing sensitivities of the employed proxies to high-frequency redox variation in the early Ediacaran ocean. Almost all proxies have multiple controlling factors, thus potentially have different sensitivities to same redox variation. For example, iron species are dependent both on basin-scale iron fluxes and benthic redox conditions (Raiswell and Canfield, 2012) and RSTEs are controlled by multiple factors such as local and global aqueous RSTE concentrations, benthic redox conditions, local organic matter loading, and sedimentation rates (Algeo and Maynard, 2004; Tribovillard et al., 2006; Scott et al., 2008; Reinhard et al., 2013; Scott and Lyons, 2012). C_{org}/P ratios depend on benthic redox conditions and organic carbon loading. One caveat to use of C_{org}/P ratios is that the organic matter must be dominantly of first-cycle marine eukaryotic algal origin; admixture of terrigenous, microbial, or recycled (i.e., eroded detrital) marine algal organic matter will weaken the robustness of redox interpretations (although inputs of terrigenous organics are not a concern for pre-Devonian strata).

High-frequency redox fluctuations are indicated by the differential responses of various trace metals to site-specific redox conditions, which is consistent with differences in their RSTE enrichment profiles (Fig. 3). For example, V is more enriched than Mo under anoxic but non-euxinic conditions, whereas both Mo and V are enriched under euxinic conditions. However, V could be preferentially scavenged under anoxic but non-euxinic conditions, resulting in high Mo contents but low V contents for euxinic shales, which has been invoked as a cause of Ni-Mo layers in shelf settings and V-rich black shales in slope-basinal settings of the early Cambrian Yangtze Platform (Fu et al., 2016). Moreover, uptake of authigenic U is initiated at the Fe(II)-Fe(III) redox boundary, whereas uptake of authigenic Mo requires the presence of H_2S (Helz et al., 1996; Algeo and Tribovillard, 2009). A Mo_{EF}-vs-U_{EF} crossplot for the 13 study sections (Fig. 4A) shows differences between shelf (U_{EF} = 1.7 (0.7–13.9); Mo_{EF} = 3.5 (1.0–11.1)), slope (U_{EF} = 3.2 (1.4–6.1); Mo_{EF} = 5.4 (0.7–18.8)), and basinal settings (U_{EF} = 2.2 (1.5–4.3); Mo_{EF} = 10.3 (3.2–37.1); note: values represent the median and 16th–84th percentile range). This pattern may be broadly redox-controlled as fluctuated suboxic to anoxic-ferruginous conditions are expected to yield relatively greater U enrichment (as seen in the shelf-slope sections), and euxinic conditions relatively greater Mo enrichment (as seen in the basinal sections; Fig. 4A).

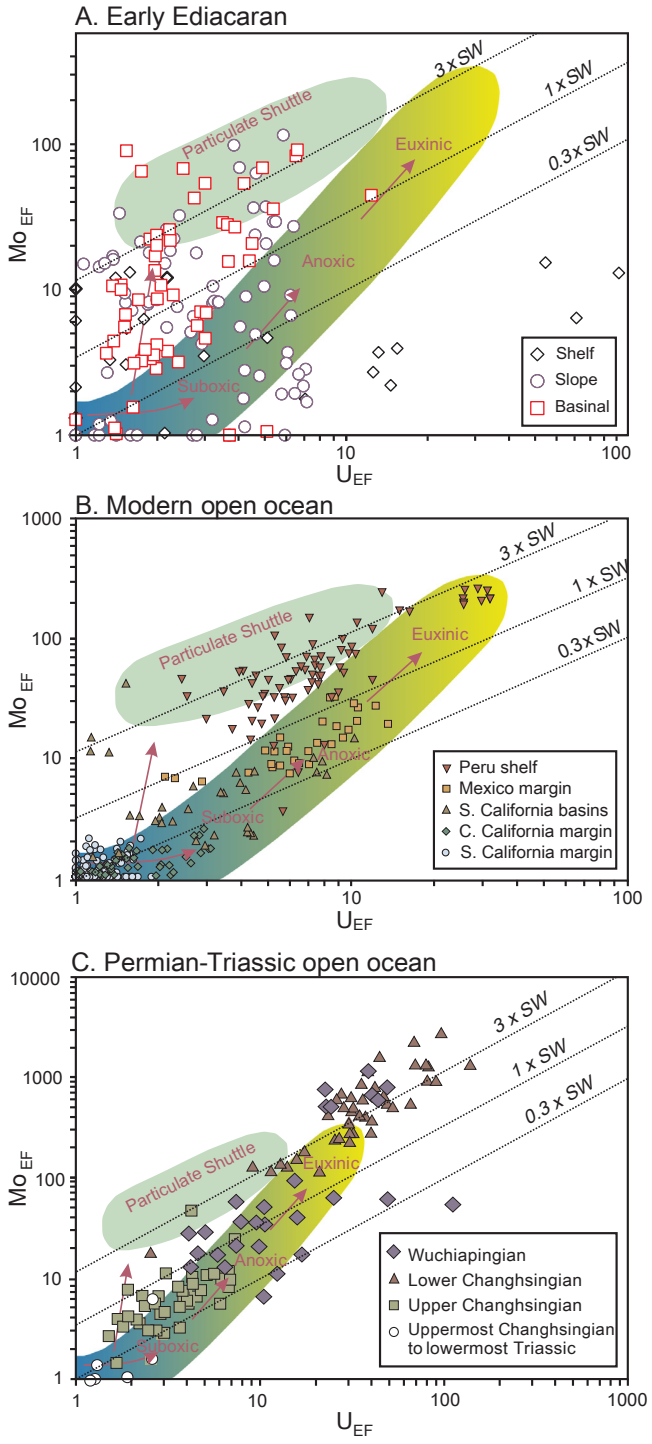

Fig. 4. Crossplots of Mo_{EF} versus U_{EF} by depositional settings for the early Ediacaran (A), compared to open-ocean sediments from the modern (B) and Permian-Triassic (C). Data sources: (A) this study and literature (Li et al., 2010; Sahoo et al., 2012, 2016; Han and Fan, 2015; Sahoo, 2015; Zhai et al., 2018); (B) Algeo and Lyons (2006) and Algeo (unpublished); and (C) Shen et al. (2013).

Our redox cross-sections show spatial and temporal variations in deepwater redox conditions along two shelf-to-basin transects across the Yangtze Block (Fig. 5). These cross-sections are characterized by spatially complex redox patterns, with multiple sections in a specific setting (e.g., slope) exhibiting section-average differences in mean redox conditions. There is also substantial evidence for high spatio-temporal variability in redox conditions including ferruginous, euxinic, suboxic, and oxic conditions across time-equivalent strata. Inner- and outer-shelf environments are characterized by fluctuations mainly between oxic and ferruginous redox conditions, whereas outer-shelf, slope, and basinal environments are characterized by fluctuations between euxinic and anoxic conditions punctuated by occasional oxic and ferruginous intervals (Fig. 5). We suggest that unstable marine redox conditions prevailed during the early Ediacaran, with large local redox shifts marked by regional heterogeneity and short-term variability. We refer to this pattern as "poikiloredox conditions" and suggest that the Siduping and Xiangtan sections serve as reference sections for this redox state.

The results for Fe species, RSTE concentrations and enrichments, and C_{org}/P ratios discussed above lead to conflicting redox interpretations for some study locales (Sections 5.1). For most locales with mixed redox results, the most likely cause may have been high-frequency "poikiloredox" variation that resulted in site-specific responses (cf. Kenig et al., 2004; Lei et al., 2017). By "high-frequency", we mean redox fluctuations at time scales shorter than the depositional interval of an individual sample; the average depositional interval was ~5 kyr based on a sample thickness of ~1 cm and an average sedimentation rate of 2 mm/kyr (see Section 2). Redox variation at time scales shorter than the depositional interval of a single sample is likely to yield a different set of responses among the utilized redox proxies than invariant, intermediate redox conditions over the same interval. At any given locale, each of the investigated proxies can exhibit substantial variability, as a consequence of which different proxies may have overlapping redox ranges even when their mean values imply different average redox conditions. Thus, the discrepancies in redox interpretations above imply that the various proxies can respond in unpredictable ways at locales that have complex redox histories (cf. Kenig et al., 2004; Lei et al., 2017; Cheng et al., 2017).

5.3. Causes of poikiloredox variation in early Ediacaran Yangtze Sea

High-frequency redox variation in slope and basinal settings of the early Ediacaran Yangtze Sea may have been related to episodic low- or high-density mass gravity flows (cf. Haughton et al., 2009). Several lines of evidence document such flows in the present study units, including: (1) occasional thin gray layers of < 1 cm thickness in black shale successions of the slope Siduping and basinal Yuanjia sections (Fig. 2; Jiang et al., 2010), and (2) slump structures and dolomitic olistostromes in the basinal Yanwutan section (Zhu et al., 2007). Another feature that is consistent with mass gravity flows is the highly variable Mo/TOC ratios (from ~0 to > 50, with clusters at both lower and higher ratios) of the two basinal sections, Wuhe and Yuanjia (in contrast to the narrow Mo/TOC ranges of shelf and slope sections; Fig. 6A and B). The lack of any systematic stratigraphic trend in Mo/TOC ratios and the markedly greater levels of Mo enrichment relative to the other study sections suggest that additional factors must have been important in the two basinal sections. We hypothesize that the highly variable RSTE concentrations and ratios of these sections result from a combination of low sedimentation rates and strong local redox variability. First, sedimentation rates are commonly low in deepwater settings, as documented, e.g., for lower Cambrian strata of the Yangtze Platform (Lehmann et al., 2007), which allows more time for authigenic RSTE uptake at the sediment-water interface. Generally slow sedimentation in the early Ediacaran Nanhua Basin may have been punctuated by episodic mass gravity flows from adjacent slopes, resulting in considerable secular variation in the sedimentation rates of basinal settings. Second, episodic mass gravity flows originating in the ocean-surface layer would have introduced dissolved oxygen to the deep Nanhua Basin, resulting in significant secular variation in redox conditions (cf. Yu et al., 2016; Cheng et al., 2017). This may have been the cause of the bimodal distribution of Mo/TOC ratios in the study units, with low values associated with intervals of more frequent mass gravity flows (characterized by higher sedimentation rates and less reducing

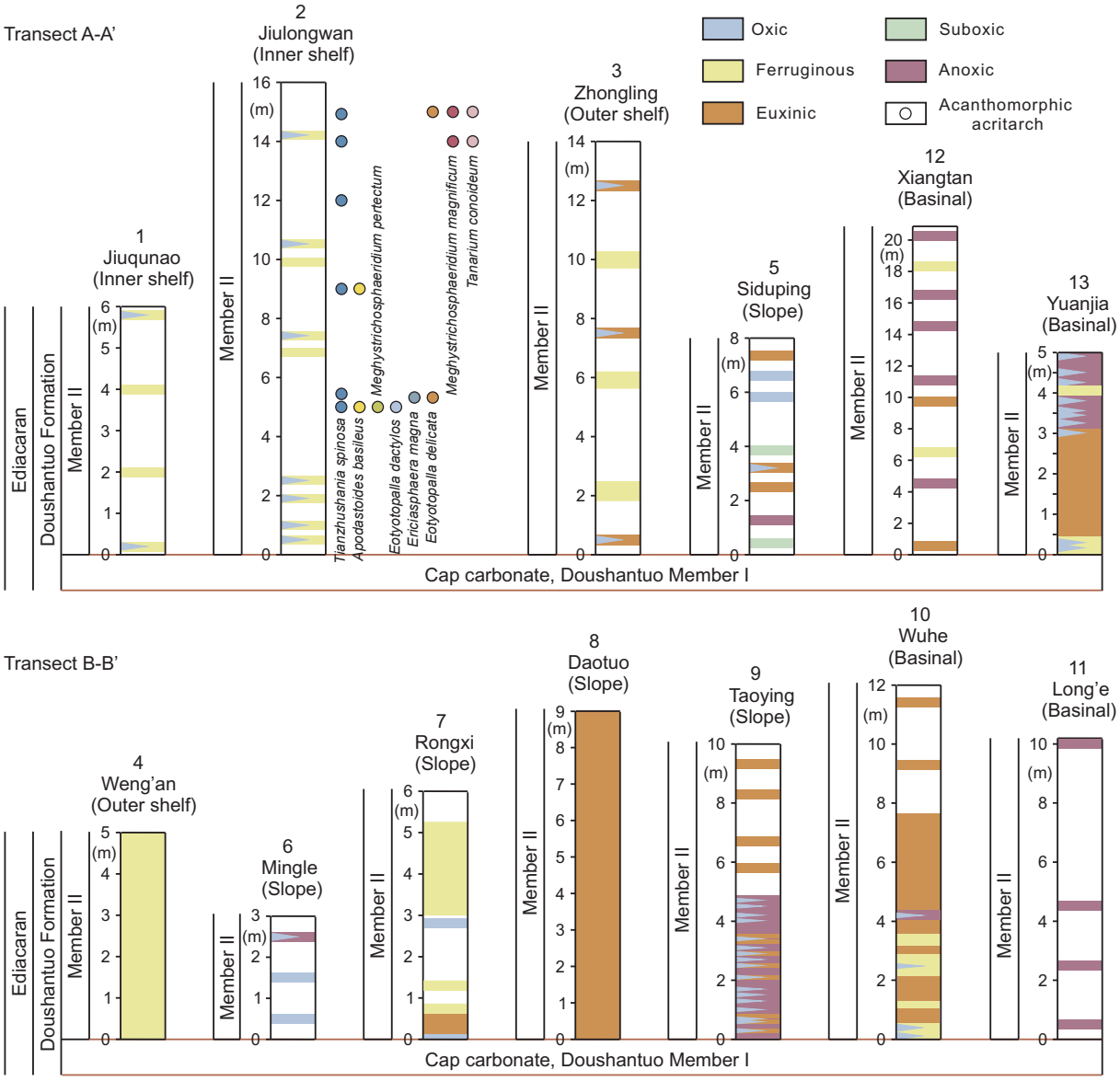

Fig. 5. A summary of redox conditions based on iron speciation, redox sensitive trace element enrichments, and framboidal pyrite data along shelf-to-basin transects A-A′ and B-B′ in Fig. 1B. Note that the suboxic and anoxic conditions are suggested by RSTE enrichments and/or framboidal pyrite without iron speciation data.

conditions, hence less RSTE uptake by the sediment), and high values associated with intervals of less frequent mass gravity flows (characterized by lower sedimentation rates and more reducing conditions, hence greater RSTE uptake by the sediment).

Oceanographic processes other than mass gravity flows also may have contributed to local redox variability. Fe-Mn particulate shuttles can accelerate the transfer of aqueous Mo (and possibly some other trace metals) to the sediment via adsorption onto sinking Fe-Mn particles that undergo redox cycling within the water column (Algeo and Tribovillard, 2009). Such particulate shuttles may have operated in the early Ediacaran Yangtze Sea, as suggested by Mo_{EF}-U_{EF} covariation patterns (Fig. 4A). Specifically, samples from shelf and slope sites show a systematic bias toward Mo enrichment relative to the modern open-ocean trend, suggesting the possible influence of an Fe-Mn-oxide particulate shuttle, suggesting a relationship to continent-margin upwelling (note: Fe-Mn-oxide particulate shuttles are known from modern upwelling zones; Scholz et al., 2013). However, samples from basinal sites fall both above and below the modern open-ocean trend, suggesting complex redox and hydrographic influences on authigenic Mo and U uptake by the sediment. One point to be emphasized is that Mo_{EF}-U_{EF} covariation in the present study units does not show a simple pattern as for modern (Fig. 4B) and Permian-Triassic (Fig. 4C) oceanic sediments.

Local redox variability also may have been influenced by dynamic changes in spatially variable watermass parameters, e.g., (1) sulfate concentrations, (2) trace-metal concentrations, or (3) organic matter production. Seawater sulfate is thought to have varied laterally across the Yangtze Block based on higher weight ratios of organic carbon to pyrite sulfur (C_{org}/S_{py}) in slope/basinal sections (mean = 39) relative to inner-shelf sections (mean = 4; Li et al., 2010). This lateral sulfate concentrations gradient was recently supported by seawater sulfate concentrations modeling work based on paired $\delta^{34}S_{CAS}$-$\delta^{34}S_{py}$ (CAS: carbonate associated sulfate) data from the upper Doushantuo Formation which recorded the major negative excursion of $\delta^{13}C$ in Ediacaran (i.e., Shuram Excursion/DOUNCE (Doushantuo Negative Carbon isotope Excursion)) (Shi et al., 2018). Aqueous trace-metal concentrations may also vary as a function of water depth owing to rapid uptake in strongly euxinic deep-water facies, as in the modern Black Sea (Algeo and Lyons, 2006; Algeo and Maynard, 2008). The present study sections show some evidence of this process as trace-metal enrichment factors

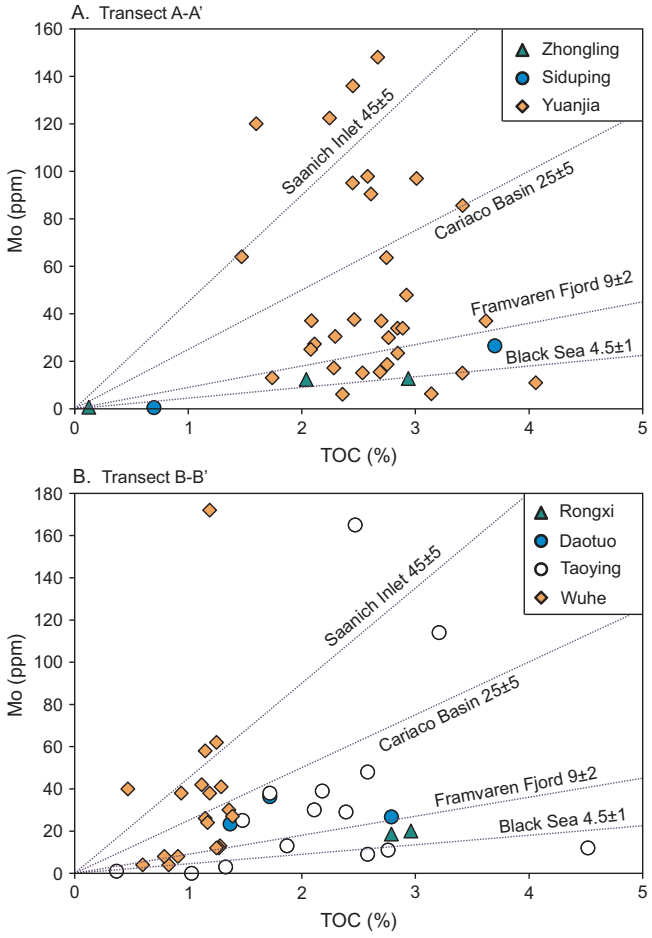

Fig. 6. Crossplots of Mo versus TOC for shale samples deposited under euxinic conditions, as inferred from Fe speciation data, and/or pyrite framboid diameters, and/or Mo > 100 ppm for transect A-A′ (A) and transect B-B′ (B) in Fig. 1B by study locale. The blue dotted lines represent the average ratios for modern restricted marine basins (Algeo and Lyons, 2006). Geochemical data are from this study and literature sources (Li et al., 2010; Sahoo et al., 2012, 2016; Zhai et al., 2018).

are lower in the deep-basinal Long'e section than in intermediate-depth sections (Fig. 3). Finally, trace-metal uptake is strongly dependent on the availability of an organic substrate, so areas with lower organic carbon sinking fluxes will take up smaller amounts of trace metals than those with higher fluxes (Algeo and Maynard, 2004; Algeo and Rowe, 2012). This factor may have been important in the early Ediacaran Yangtze Sea owing to locally low TOC values (< 0.5%, as in some samples from Jiulongwan, Zhongling, and Siduping; Fig. 3).

6. Conclusions

Fe speciation data, trace and major elemental abundances, and C_{org}/P ratios were analyzed as needed in black shales from the inner-shelf Jiulongwan, outer-shelf Zhongling, slope Siduping and Mingle, and basinal Yuanjia and Long'e sections. These new data, integrated with existing data from these sections and seven other correlative sections of the Yangtze Platform (inner-shelf Jiuqunao, outer-shelf Weng'an, slope Rongxi, Daotuo and Taoying, and basinal Wuhe and Xiangtan), allow an understanding of basin-scale (shelf to basin transects) redox conditions of time equivalent environments. We find that conflicting redox interpretations based on these proxies are common for study sections, which can be explained by high spatiotemporal variability in redox conditions including ferruginous, euxinic, suboxic, and oxic conditions in the early Ediacaran ocean. Inner- and outer-shelf environments are characterized by fluctuations in oxic and ferruginous redox conditions, while outer-shelf, slope, and basinal environments are characterized largely by euxinic and anoxic fluctuations, with occasional oxic and ferruginous episodes. Thus, marine redox conditions were characterized by strong spatio-temporal variability (="poikiloredox conditions"), which may reflect the transitional state of the Ediacaran ocean between the dominantly anoxic conditions of earlier oceans and the dominantly oxic conditions of Phanerozoic oceans (cf. Cheng et al., 2017; Planavsky et al., 2018). Finally, our study documents differential responses of multiple redox proxies (e.g., iron species, RSTE concentrations and enrichments, and C_{org}/P ratios) to high-frequency variation of oceanic redox conditions in the early Ediacaran Yangtze Sea. More broadly, this work highlights potential pitfalls basing broad-scale marine redox reconstructions on a single redox proxy or section.

Acknowledgments

This study was supported by National Key R&D Program of China (grant 2016YFA0601100), NSFC-RCUK_NERC Program (grant 41661134048), NSFC Program (grant 41703008) and the China University of Geosciences-Wuhan (SKL-GPMR program GPMR201705). Research by TJA is supported by the U.S. National Science Foundation (Sedimentary Geology and Paleobiology program, grant No. EAR-1053449), the NASA Exobiology program (grant No. NNX13AJ1IG), and the China University of Geosciences-Wuhan (SKL-GPMR program GPMR201301, and SKL-BGEG program BGL201407). NJP acknowledges support from the Packard Foundation.

Appendix A. Supplementary data

Supplementary data associated with this article can be found, in the online version, at http://dx.doi.org/10.1016/j.precamres.2018.04.012.

References

Algeo, T.J., Ingall, E., 2007. Sedimentary C_{org}:P ratios, paleocean ventilation, and Phanerozoic atmospheric p_O2. Palaeogeogr. Palaeoclimatol. Palaeoecol. 256, 130–155.
Algeo, T.J., Lyons, T.W., 2006. Mo–total organic carbon covariation in modern anoxic marine environments: implications for analysis of paleoredox and paleohydrographic conditions. Paleoceanography 21 (1).
Algeo, T.J., Maynard, J.B., 2004. Trace-element behavior and redox facies in core shales of Upper Pennsylvanian Kansas-type cyclothems. Chem. Geol. 206, 289–318.
Algeo, T.J., Maynard, J.B., 2008. Trace-metal covariation as a guide to water-mass conditions in ancient anoxic marine environments. Geosphere 4, 872–887.
Algeo, T.J., Rowe, H., 2012. Paleoceanographic applications of trace-metal concentration data. Chem. Geol. 324, 6–18.
Algeo, T.J., Tribovillard, N., 2009. Environmental analysis of paleoceanographic systems based on molybdenum–uranium covariation. Chem. Geol. 268, 211–225.
Bristow, T.F., Kennedy, M.J., Derkowski, A., Droser, M.L., Jiang, G.Q., Creaser, R.A., 2009. Mineralogical constraints on the paleoenvironments of the Ediacaran Doushantuo Formation. In: Proceedings of the National Academy of Sciences (U.S.A.), pp. 13190–13195.
Canfield, D.E., Raiswell, R., Westrich, J.T., Reaves, C.M., Berner, R.A., 1986. The use of chromium reduction in the analysis of reduced inorganic sulfur in sediments and shales. Chem. Geol. 54, 149–155.
Cheng, M., Li, C., Zhou, L., Feng, L.J., Algeo, T.J., Zhang, F.F., Romaniello, S., Jin, C.S., Ling, H.F., Jiang, S.Y., 2017. Transient deep-water oxygenation in the early Cambrian Nanhua Basin, South China. Geochim. Cosmochim. Acta 210, 42–58.
Clarkson, M., Poulton, S., Guilbaud, R., Wood, R., 2014. Assessing the utility of Fe/Al and Fe-speciation to record water column redox conditions in carbonate-rich sediments. Chem. Geol. 382, 111–122.
Condon, D., Zhu, M., Bowring, S., Wang, W., Yang, A., Jin, Y., 2005. U-Pb ages from the Neoproterozoic Doushantuo Formation, China. Science 308, 95–98.
Emerson, S.R., Huested, S.S., 1991. Ocean anoxia and the concentrations of molybdenum and vanadium in seawater. Mar. Chem. 34, 177–196.
Filippelli, G.M., 2002. The global phosphorus cycle. In: Kohn, M.J., Rakovan, J., Hughes, J.M. (Eds.), Phosphates: Geochemical, Geobiological, and Materials Importance. Reviews in Mineralogy and Geochemistry, pp. 391–425.
Fu, Y., Dong, L., Li, C., Qu, W., Pei, H., Qiao, W., Shen, B., 2016. New Re-Os isotopic constrains on the formation of the metalliferous deposits of the Lower Cambrian Niutitang formation. J. Earth Sci. 27, 271–281.
Gregory, D.D., Lyons, T.W., Large, R.R., Jiang, G., Stepanov, A.S., Diamond, C.W., Figueroa, M.C., Olin, P., 2017. Whole rock and discrete pyrite geochemistry as complementary tracers of ancient ocean chemistry: an example from the

Neoproterozoic Doushantuo Formation, China. Geochim. Cosmochim. Acta 216, 201–220.
Han, T., Fan, H., 2015. Dynamic evolution of the Ediacaran ocean across the Doushantuo Formation, South China. Chem. Geol. 417, 261–272as.
Haughton, P., Davis, C., McCaffrey, W., Barker, S., 2009. Hybrid sediment gravity flow deposits–classification, origin and significance. Mar. Pet. Geol. 26, 1900–1918.
Helz, G.R., Miller, C.V., Charnock, J.M., Mosselmans, J.F.W., Pattrick, R.A.D., Garner, C.D., Vaughan, D.J., 1996. Mechanism of molybdenum removal from the sea and its concentration in black shales: EXAFS evidence. Geochim. Cosmochim. Acta 60, 3631–3642.
Huang, J., Chu, X., Lyons, T.W., Planavsky, N.J., Wen, H., 2013. A new look at saponite formation and its implications for early animal records in the Ediacaran of South China. Geobiology 11, 3–14.
Ingall, E.D., Bustin, R., Van Cappellen, P., 1993. Influence of water column anoxia on the burial and preservation of carbon and phosphorus in marine shales. Geochim. Cosmochim. Acta 57, 303–316.
Jiang, G.Q., Wang, X., Shi, X., Zhang, S., Xiao, S., Dong, J., 2010. Organic carbon isotope constraints on the dissolved organic carbon (DOC) reservoir at the Cryogenian-Ediacaran transition. Earth Planet. Sci. Lett. 299, 159–168.
Jiang, G.Q., Shi, X.Y., Zhang, S.H., Wang, Y., Xiao, S.H., 2011. Stratigraphy and paleogeography of the Ediacaran Doushantuo Formation (ca. 635–551 Ma) in South China. Gondwana Res. 19, 831–849.
Kenig, F., Hudson, J.D., Sinninghe Damsté, J.S., Popp, B.N., 2004. Intermittent euxinia: reconciliation of a Jurassic black shale with its biofacies. Geology 32, 421–424.
Lehmann, B., Nägler, T.F., Holland, H.D., Wille, M., Mao, J., Pan, J., Ma, D., Dulski, P., 2007. Highly metalliferous carbonaceous shale and Early Cambrian seawater. Geology 35, 535–540.
Lei, L.D., Shen, J., Li, C., Algeo, T.J., Chen, Z.Q., Feng, Q.L., Cheng, M., Jin, C.S., Huang, J.H., 2017. Controls on regional marine redox evolution during Permian-Triassic transition in South China. Palaeogeogr. Palaeoclimatol. Palaeoecol. 486, 17–32.
Li, C., Love, G.D., Lyons, T.W., Fike, D.A., Sessions, A.L., Chu, X., 2010. A stratified redox model for the Ediacaran ocean. Science 328, 80–83.
Li, C., Planavsky, N.J., Shi, W., Zhang, Z., Zhou, C., Cheng, M., Tarhan, L.G., Luo, G., Xie, S., 2015a. Ediacaran marine redox heterogeneity and early animal ecosystems. Sci. Rep. 5, 17097.
Li, C., Cheng, M., Algeo, T.J., Xie, S., 2015b. A theoretical prediction of chemical zonation in early oceans (> 520 Ma). Sci. China Earth Sci. 58, 1901–1909.
Lyons, T.W., Severmann, S., 2006. A critical look at iron paleoredox proxies: new insights from modern euxinic marine basins. Geochim. Cosmochim. Acta 70, 5698–5722.
Lyons, T.W., Reinhard, C.T., Planavsky, N.J., 2014. The rise of oxygen in Earth's early ocean and atmosphere. Nature 506, 307–315.
McFadden, K.A., Xiao, S., Zhou, C., Kowalewski, M., 2009. Quantitative evaluation of the biostratigraphic distribution of acanthomorphic acritarchs in the Ediacaran Doushantuo Formation in the Yangtze Gorges area, South China. Precambrian Res. 173, 170–190.
McLennan, S.M., 2001. Relationships between the trace element composition of sedimentary rocks and upper continental crust. Geochem. Geophys. Geosyst. 2, 203–236.
Miller, A.J., Strauss, J.V., Halverson, G.P., Macdonald, F.A., Johnston, D.T., Sperling, E.A., 2017. Tracking the onset of Phanerozoic-style redox-sensitive trace metal enrichments: new results from basal Ediacaran post-glacial strata in NW Canada. Chem. Geol. 457, 24–37.
Och, L.M., Cremonese, L., Shields-Zhou, G.A., Poulton, S.W., Struck, U., Ling, H., Li, D., Chen, X., Manning, C., Thirlwall, M., Strauss, H., Zhu, M., 2016. Palaeoceanographic controls on spatial redox distribution over the Yangtze Platform during the Ediacaran-Cambrian transition. Sedimentology 63, 378–410.
Planavsky, N.J., Slack, J.F., Cannon, W.F., O'Connell, B., Terry-Tang, Y., Asael, D., Jackson, J.C., Hardisty, D.S., Lyons, T.W., Bekker, A., 2018. Evidence for episodic oxygenation in a weakly redox-buffered deep mid-Proterozoic ocean. Chem. Geol. http://dx.doi.org/10.1016/j.chemgeo.2018.03.028.
Poulton, S.W., Canfield, D.E., 2005. Development of a sequential extraction procedure for iron: implications for iron partitioning in continentally derived particulates. Chem. Geol. 214, 209–221.
Poulton, S.W., Canfield, D.E., 2011. Ferruginous conditions: a dominant feature of the ocean through Earth's history. Elements 7, 107–112.
Raiswell, R., Canfield, D.E., 1998. Sources of iron for pyrite formation in marine sediments. Am. J. Sci. 298, 219–245.
Raiswell, R., Canfield, D.E., 2012. The iron biogeochemical cycle past and present. Geochem. Perspect. 1, 1–220.
Reinhard, C.T., Planavsky, N.J., Robbins, L.J., Partin, C.A., Gill, B.C., Lalonde, S.V., Bekker, A., Konhauser, K.O., Lyons, T.W., 2013. Proterozoic ocean redox and biogeochemical stasis. In: Proceedings of the National Academy of Sciences (U.S.A.), pp. 5357–5362.
Reinhard, C.T., Planavsky, N.J., Gill, B.C., Ozaki, K., Robbins, L.J., Lyons, T.W., Fischer, W.W., Wang, C., Cole, D.B., Konhauser, K.O., 2017. Evolution of the global phosphorus cycle. Nature 541, 386–389.
Ruttenberg, K.C., 2003. The global phosphorus cycle. In: Holland, H.D., Turekian, K.K. (Eds.), Biogeochemistry. Treatise on Geochemistry, pp. 585–643.
Sahoo, S.K., Planavsky, N.J., Kendall, B., Wang, X., Shi, X., Scott, C., Anbar, A.D., Lyons, T.W., Jiang, G., 2012. Ocean oxygenation in the wake of the Marinoan glaciation. Nature 489, 546–549.
Sahoo, S., Planavsky, N., Jiang, G., Kendall, B., Owens, J., Wang, X., Shi, X., Anbar, A., Lyons, T., 2016. Oceanic oxygenation events in the anoxic Ediacaran ocean. Geobiology 14, 457–468.
Sahoo, S.K., 2015. Ediacaran ocean redox evolution (Ph. D thesis). University of Nevada, Las Vegas.
Scheller, E.L., Dickson, A.J., Canfield, D.E., Korte, C., Kristiansen, K.K., Dahl, T.W., 2017. Ocean redox conditions between the Snowballs–geochemical constraints from Arena Formation, East Greenland. Precambrian Res. http://dx.doi.org/10.1016/j.precamres.2017.12.009.
Scholz, F., McManus, J., Sommer, S., 2013. The manganese and iron shuttle in a modern euxinic basin and implications for molybdenum cycling at euxinic ocean margins. Chem. Geol. 355, 56–68.
Scott, C., Lyons, T.W., Bekker, A., Shen, Y., Poulton, S.W., Chu, X., Anbar, A.D., 2008. Tracing the stepwise oxygenation of the Proterozoic ocean. Nature 452, 456–459.
Scott, C., Lyons, T.W., 2012. Contrasting molybdenum cycling and isotopic properties in euxinic versus non-euxinic sediments and sedimentary rocks: refining the paleoproxies. Chem. Geol. 324, 19–27.
Shen, J., Algeo, T.J., Feng, Q., Zhou, L., Feng, L., Zhang, N., Huang, J., 2013. Volcanically induced environmental change at the Permian-Triassic boundary (Xiakou, Hubei Province, South China): related to West Siberian coal-field methane releases? J. Asian Earth Sci. 75, 95–109.
Shi, W., Li, C., Luo, G., Huang, J., Algeo, T.J., Jin, C., Zhang, Z., Cheng, M., 2018. Sulfur isotope evidence for transient marine-shelf oxidation during the Ediacaran Shuram Excursion. Geology 46, 267–270.
Slotznick, S.P., Eiler, J.M., Fischer, W.W., 2018. The effects of metamorphism on iron mineralogy and the iron speciation redox proxy. Geochim. Cosmochim. Acta 224, 96–115.
Sperling, E.A., Wolock, C.J., Morgan, A.S., Gill, B.C., Kunzmann, M., Halverson, G.P., Macdonald, F.A., Knoll, A.H., Johnston, D.T., 2015. Statistical analysis of iron geochemical data suggests limited late Proterozoic oxygenation. Nature 523, 451–454.
Tribovillard, N., Algeo, T.J., Lyons, T., Riboulleau, A., 2006. Trace metals as paleoredox and paleoproductivity proxies: an update. Chem. Geol. 232, 12–32.
Tyson, R.V., Pearson, T.H., 1991. Modern and ancient continental shelf anoxia: an overview. In: Tyson, R.V., Pearson, T.H. (Eds.), Modern and Ancient Continental Shelf Anoxia. Geological Society of London Special Publication, pp. 1–24.
Wang, J., Li, Z., 2003. History of Neoproterozoic rift basins in South China: implications for Rodinia break-up. Precambrian Res. 122, 141–158.
Wang, L., Shi, X., Jiang, G., 2012. Pyrite morphology and redox fluctuations recorded in the Ediacaran Doushantuo Formation. Palaeogeogr. Palaeoclimatol. Palaeoecol. 333–334, 218–227.
Ye, Y.T., Wu, C.D., Zhai, L.N., An, Z.Z., 2017. Pyrite morphology and episodic euxinia of the Ediacaran Doushantuo Formation in South China. Sci. China Earth Sci. 60, 102–113.
Yu, W.C., Algeo, T.J., Du, Y.S., Maynard, J.B., Zhou, Q., Wang, P., Yuan, L.J., Xu, Y., Guo, H., 2016. Genesis of Cryogenian Datangpo manganese deposit: hydrothermal metal inputs and episodic post-glacial ventilation of Nanhua Basin, South China. Palaeogeogr. Palaeoclimatol. Palaeoecol. 459, 321–337.
Yuan, X., Chen, Z., Xiao, S., Zhou, C., Hua, H., 2011. An early Ediacaran assemblage of macroscopic and morphologically differentiated eukaryotes. Nature 470, 390–393.
Zhai, L., Wu, C., Ye, Y., Zhang, S., An, Z., 2018. Marine redox variations during the Ediacaran-Cambrian transition on the Yangtze Platform, South China. Geol. J. 53, 58–79.
Zhang, S., Evans, D.A.D., Li, H., Wu, H., Jiang, G., Dong, J., Zhao, Q., Raub, T.D., Yang, T., 2013. Paleomagnetism of the late Cryogenian Nantuo Formation and paleogeographic implications for the South China Block. J. Asian Earth Sci. 72, 164–177.
Zhou, C., Xie, G., McFadden, K., Xiao, S., Yuan, X., 2007. The diversification and extinction of Doushantuo-Pertatataka acritarchs in South China: causes and biostratigraphic significance. Geol. J. 42, 229–262.
Zhu, M., Zhang, J., Yang, A., 2007. Integrated Ediacaran (Sinian) chronostratigraphy of South China. Palaeogeogr. Palaeoclimatol. Palaeoecol. 254, 7–61.